

Transition in the Acid-Base Component of Surface Free Energy of Ice upon the Premelting of its Second Molecular Bilayer

Nathaniel Orndorf, Saranshu Singla, Ali Dhinojwala*

Department of Polymer Science, The University of Akron, Akron, OH 44325

(Dated: May 9, 2020)

Molecular disordering of the ice surface occurs below the bulk melting temperature of 273 K, termed surface premelting. The top-most molecular layer begins gradually premelting at 200 K, and has been linked to its low coefficient of friction through an increase in molecular mobility. The second molecular bilayer premelts around 257 K, but no study has linked this transition to a change in any macroscopic phenomena. Here, we show that the thermodynamic work of adhesion between polydimethylsiloxane and ice changes abruptly at 257 K. Surface-sensitive spectroscopy indicates that the transition arises from changes of the ice surface. We show that this transition is due to a decrease in the acid-base component of the surface free energy of ice by 13 ± 2 mJ/m² at 257 K. The change in surface energy provides a possible explanation for a variety of unexplained phenomena seen across the literature including ice adhesion, friction, and the morphology of snowflakes.

Understanding how the molecular structure at the surface of solids dictates macroscopic properties such as surface free energy, adhesion, and friction has been a long standing problem in interfacial science and has applications in many areas. One particular area of high interest, but of which little is understood, is that of the surface of ice. Detailed knowledge on the surface of ice is important at all length scales, from antifreeze proteins keeping organisms alive well below freezing [1] to sliding glaciers forming landscapes [2]. The properties of ice are important in understanding the history of our planet [3] and the solar system [4,5]. From an application perspective, ice accretion and adhesion to aircraft [6], wind turbines [7], solar panels [8], and power lines [9] decreases energy efficiency and presents dangerous situations. It is likely that climate change will cause icing events to shift in latitude, showing potential for these problems to become common in new locations [10]. Understanding friction on ice has implications in the grip of winter automobile tires and shoe soles [11,12]. Unraveling the mechanism behind antifreeze proteins will advance technologies in agriculture and food preservation [1]. In all of these examples, it is crucial to understand the surface and interfacial interactions of ice, both in terms of understanding our universe and advancing new materials and technologies that will increase the standard of living of people worldwide.

The surface of ice, or ice-air interface, has been increasingly studied since Michael Faraday first postulated its surface premelting in 1850 [13]. Since then, it has commonly been shown by several different techniques that the surface of ice behaves 'liquid-like' below the bulk melting temperature of 273 K [14]. The technique most sensitive to surfaces and interfaces is sum frequency generation spectroscopy (SFG), which was first introduced in practice by Zhu *et al.* in 1987 [15]. By

overlapping a beam with a fixed frequency in the visible range ω_{vis} and a beam with a tunable frequency in the infrared range ω_{IR} , the resulting SFG intensity at the sum of the beams' frequency $\omega_{SFG} = \omega_{vis} + \omega_{IR}$ provides information on the ordering of molecules and the strength of interactions to depth of a few molecular layers [16,17]. SFG has been used to identify two specific premelting transitions of the ice surface. In 2001, Wei *et al.* showed that the free O-H of the topmost molecular layer becomes increasingly disordered as the temperature is increased from 200 K [18,19]. More recently, Sanchez *et al.* showed that there is a sharp transition in the bonded O-H peak location around 257 K in both experiments and molecular simulations, which was attributed to the premelting of the second molecular bilayer [20]. In the same study, they also confirmed that the intensity of the free O-H peak decreases with increasing temperature, but there is no shift in the free O-H peak location, showing that this transition has no major structural effects on the topmost layer. A perspective by Yamaguchi gives a more detailed history of ice studied by SFG [21].

Such studies are being used to begin to understand the mechanism behind ice friction [22]. Likewise, an attempt to link premelting to the shear adhesion strength of ice demonstrated that the premelt layer facilitates sliding [23]. But, through a collection of data across the literature, it has been shown that mechanical ice adhesion tests have large uncertainties across several orders of magnitude [24]. This disagreement is likely due to energy dissipation in deforming the materials, rendering mechanical adhesion tests imprecise when aiming to extract thermodynamic quantities. These studies link the gradual disordering of the topmost molecular layer of the ice surface to gradual changes in the mechanical mobility of the surface molecules, resulting in low friction and sliding

resistance [25]. However, a link between the precise premelting of the second molecular bilayer and surface properties has yet to be shown. Any reconfiguration of the molecules on the surface of ice likely results in a change in its surface free energy. The surface energy of medium i , γ_i^{tot} , can be written as a sum of energies of different interactions, namely the Lifshitz-van der Waals (LW) and acid-base (AB) interactions [26]

$$\gamma_i^{tot} = \gamma_i^{LW} + \gamma_i^{AB}. \quad (1)$$

The surface energy of ice has been measured by contact angles of various liquids on ice [27–29], the contact angle of water at grain boundaries [30], homogeneous nucleation rates [31], and molecular simulations [32]. These studies generally result in $\gamma_{ice}^{tot} \sim 100$ mJ/m², but precise determination of the surface free energy is difficult. Furthermore, no study has adequately examined the surface energy of ice over its premelting transitions. In 1970, Adamson *et al.* measured the contact angle of carbon disulfide on ice from 225 to 270 K, but no transition was found [27]. Nearly two decades later, van Oss *et al.* used various probe liquids to measure γ_{ice}^{AB} to be 60.4 and 48.0 mJ/m² at 253 and 265 K respectively, but they assumed a linear trend in γ_{ice}^{AB} in order to extrapolate their results to 273 K [29].

Here, we use Johnson, Kendall, and Roberts’s theory of elastic adhesion (JKR) [33] to measure the thermodynamic work of adhesion between polydimethylsiloxane (PDMS) and ice. The thermodynamic work of adhesion is defined as the amount of reversible energy needed to separate an interface between media i and j and create two surfaces, expressed by the Dupr’e Equation

$$W_a = \gamma_i^{tot} + \gamma_j^{tot} - \gamma_{ij}^{tot} \quad (2)$$

where γ_{ij}^{tot} is the total interfacial free energy between media i and j [34]. Thus, measuring the work of adhesion allows us to make inferences on the surface energy of ice. The JKR model was derived for the contact between two elastic spheres, but by taking one sphere in the limit of infinite radius and infinite elastic modulus, the well-known JKR equation expresses the radius of the contact circle a between a hard, flat plane and an elastic sphere of radius R and modulus E by

$$a^3 = \frac{9R}{16E} \left[P + 3\pi RW_a + \sqrt{6\pi RPW_a + (3\pi RW_a)^2} \right]. \quad (3)$$

In the simplifying case that the load P between the sphere and plane is negligible,

$$a^3 = \frac{27\pi}{8} \frac{R^2}{E} W_a. \quad (4)$$

Thus, by measuring the contact radius formed between an elastic spherical cap of known radius and elastic modulus and a flat piece of ice at zero load, the thermodynamic work of adhesion can be extracted.

In 1981, Roberts and Richardson conducted similar ‘touch on’ experiments on ice with a large 1.8 cm diameter polyisoprene hemisphere [35]. They saw a drastic increase in the contact radius as the temperature approached 273 K. Rather than a true thermodynamic increase in W_a , this was attributed to the formation of a

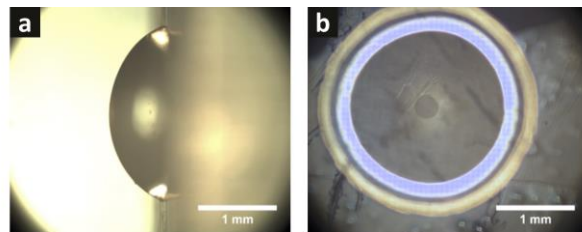


FIG. 1. Side view of a PDMS spherical cap (a). When the spherical side is placed in contact with ice, the contact spot can clearly be seen by viewing through the flat side of the cap (b).

capillary bridge of the premelt layer between the hemisphere and the ice—a claim which is supported by a drop in friction and pull-off adhesion at the same temperature. They also noticed circular marks left on the ice from where the contact had been, which were more apparent with increasing dwell time, load, or temperature. Due to the capillary bridging resulting in inaccurate measurements of W_a , their study does not allow for conclusions about the surface free energy of ice to be drawn.

To explore these effects with greater accuracy, we fabricated much smaller (≈ 1 mm radius) PDMS spherical caps of elastic modulus 1.9 MPa as previously described [36]. Because of its low elastic modulus and surface energy, PDMS is often the host material in low ice adhesion surfaces [37–39]. However, no work has been done to explicitly study the ice-PDMS interfacial interactions. Ice was frozen in solvent cleaned ice cube trays from purified water (Milipore Filtration System, $\rho = 18.2$ M Ω cm). Once frozen, the ice cubes were removed from the tray and frozen onto aluminum plates for handling. To ensure a smooth surface, the ice was microtomed using cuts as small as 1 μ m thick. Both the freezing and JKR experiments were conducted in a walk-in freezer, which was equilibrated for at least 24 hours prior to starting the experiments.

The spherical side of a PDMS cap was carefully placed on the ice surface using tweezers, and the contact was viewed through the flat side of the cap using a microscope. Images were recorded (shown in Fig. 1), which were used

to measure the contact radius a and cap radius R . These measurements were repeated about five times at different locations on the ice in order to calculate an average and standard error for a single cap, and several caps of various radii were used. The experiment was replicated at several temperatures in the range of 243 to 268 K. Because the elastic modulus of the PDMS was measured at room temperature, the elastic modulus at the lower temperatures was calculated by scaling according to the affine model, given by $\frac{E(T_1)}{E(T_2)} = \frac{T_1}{T_2}$ [40].

Figure 2 displays the measured work of adhesion between PDMS and ice at various temperatures. A sigmoidal fit shows a transition from 116 ± 2 to 73 ± 3 mJ/m^2

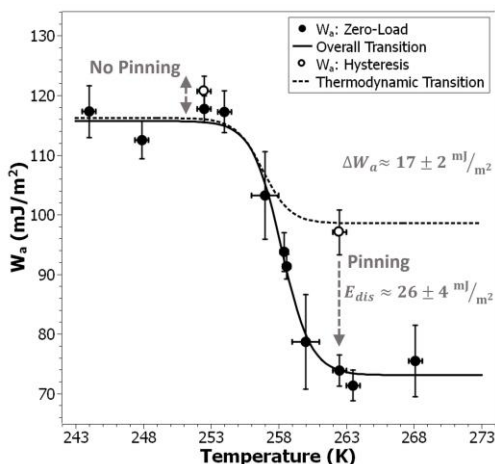


FIG. 2. Measured work of adhesion between PDMS and ice. Both lines are logistical function fits.

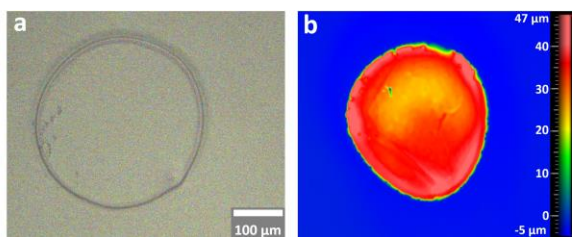


FIG. 3. A mark the same shape as the contact area left on the ice surface (a). Optical profilometry of a surface replica (opposite in height) from a different mark confirms that the marks are impressions into the ice surface (b).

when heated above 258.4 ± 0.2 K, which is interestingly similar to the temperature at which the second molecular bilayer of the ice surface premelts [20]. When the small weight of the caps ≈ 5 mN is taken into account, Equation 3 calculates ~ 5 mJ/m^2 lower than the zero-load

approximation shown in Figure 2, but the difference in the measurements before and after the transition $\Delta W_a = 43 \pm 4$ mJ/m^2 is identical. Similar to Roberts and Richardson, we noticed circular marks left on the ice after longer dwell times, much more readily at temperatures above 258 K. Optical profilometer measurements of replicas of the ice surface (opposite in height) shown in Figure 3 confirm that these circular marks are impressions left in the ice surface in the shape of the contact area. The only temperature for which these impressions occurred during the time frame of a measurement was 268 K, resulting in a larger apparent contact than the value of interest. The width of the impression circle on the surface of ice is measured to be ≈ 9 μm , which is subtracted from the measured contact radii to calculate the true contact radius at 268 K.

Because the work of adhesion is dependent on the initial state interface (ice-PDMS) and the final state surfaces (PDMS-air and ice-air), we must also understand how the PDMS surface and ice-PDMS interface change with temperature. PDMS films of 200 nm thickness were made by spin-coating (70 s at 2000 rpm) 4 wt.% PDMS (Gelest, vinyl terminated, $M_w = 28000$) in Hexane (Sigma-Aldrich, $\geq 99\%$ purity) onto sapphire prisms. The SFG spectra at various temperatures were taken of the PDMS surface, and water was frozen next to the PDMS film to measure the spectra of the ice-PDMS interface, both of which are shown in Figure 4. It is evident that the SFG spectra of the PDMS surface do not change in this temperature range. The peaks at 2911.5 ± 0.7 and 2965.4 ± 0.6 cm^{-1} are assigned to the symmetric and asymmetric CH_3 stretch modes, respectively [41–44]. The 2910 cm^{-1} PDMS peak is present against water but not ice, which could be due to chemical interactions between the CH_3 groups and ice or simply due to the more intense SFG peaks from ice overshadowing those of PDMS. The ice-PDMS spectra show three peaks: a peak at 3135 ± 3 cm^{-1} corresponding to the O–H stretch mode bonded in the ice lattice (four hydrogen bonds) [18, 19], a broad peak centered at 3410 ± 6 cm^{-1} corresponding to lower coordination hydrogen bonds (less than four) [45], and a peak at 3708 ± 17 cm^{-1} corresponding to the free O–H stretch mode [18, 19]. A signal from the buried sapphire-PDMS interface produces higher uncertainty and noise in the 3700 cm^{-1} peak. The 3135 cm^{-1} peak appears at a lower wavenumber than that of the ice surface [18–20], but, unlike the ice surface [20], this peak shows no shift in either the peak center or the first moment with a change in temperature between 243 and 268 K. No shift in this peak indicates that there is no premelting transition in this temperature range. It could be the case that the premelting of the second bilayer is shifted to either higher or lower temperatures. In either case, it is evident that the measured transition in the work

of adhesion does not arise from structural changes on the PDMS surface or the ice-PDMS interface. Thus, by reasoning analogous to Equation 2, we conclude that the transition in the work of adhesion is due to changes on the ice surface, specifically at the same temperature at which the second molecular bilayer premelts. This change can arise from a thermodynamic change in γ_{ice}^{tot} , from adhesion hysteresis in the contact line advancing or receding kinetics, or a combination of both.

To simply check for hysteresis, we applied a higher load to the cap with the tweezers, released the load, and measured the contact area after it returned to stability. Repeating the same loading on a simple laboratory scale resulted in a highly variable applied load between 10 and 50 mN. Using this technique at 253 K, the contact area returns to what it was at zero-load, showing that there is no adhesion hysteresis below 258 K. Thus, $W_a = 116 \pm 2$ mJ/m² below 258 K is suspected to be a true thermodynamic value.

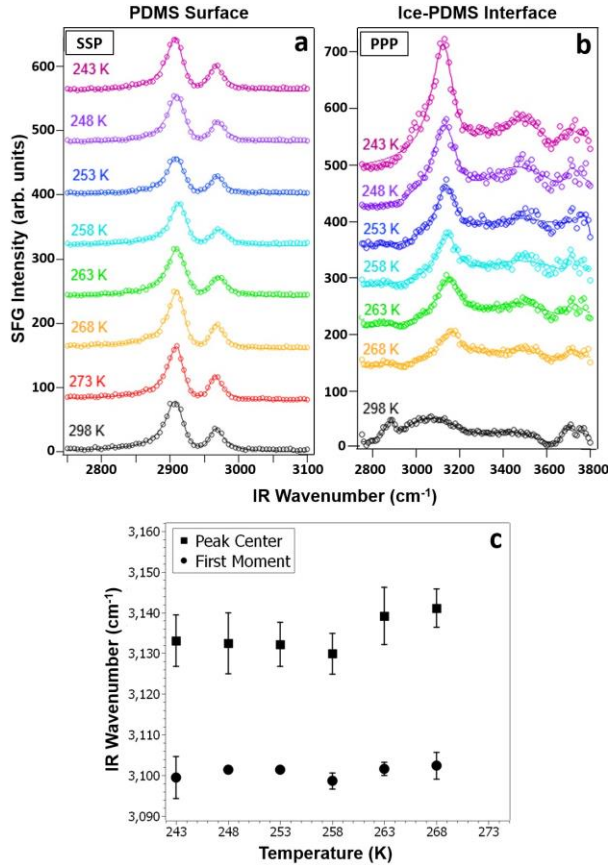


FIG. 4. Representative SFG spectra of the PDMS surface (a) and the ice-PDMS interface (b) at various temperatures. The solid lines are Lorentzian peak fits. The ice-PDMS interface spectra show no shift in the center or first moment of the bonded O-H peak location (c).

Conversely, after applying a higher load at 263 K, the contact area does not return to that of zero-load. Instead, the contact area returns to the value corresponding to 99 mJ/m². This shows that above 258 K, the true thermodynamic value is $W_a \leq 99$ mJ/m². While there was a high variance in the applied load, the contact area repeatedly returned to the same value, suggesting that the true thermodynamic value is around 99 mJ/m² above 258 K. The pinning at 73 mJ/m² suggests that there is 26 ± 4 mJ/m² of energy dissipation on the ice surface when second bilayer is premelted, which restricts the advancing of the contact line to its thermodynamic position. Thus, we conclude that the rest of the change arises from thermodynamic effects.

To explore this thermodynamic change, we fit the thermodynamic data with a sigmoidal curve, which shows a transition from 116 ± 1 to 99 ± 2 mJ/m² when heated above 257.0 ± 0.1 K. This thermodynamic transition lies closer to the premelting transition temperature, and consists of $\Delta W_a = 17 \pm 2$ mJ/m². Our SFG experiments conclude that $\Delta W_a \approx \Delta \gamma_{ice}^{tot}$, where $\Delta \gamma_{ice}^{tot}$ is the difference in γ_{ice}^{tot} before and after the transition at 257 K. Similar to most polymers, the surface energy of PDMS increases about 0.5 mJ/m² when cooled by 10 K [46]. Because no transition is present at the ice-PDMS interface, we expect $\gamma_{ice-PDMS}$ to behave the same. Using Equation 2, we calculate $\Delta \gamma_{ice}^{tot} \approx 16 \pm 2$ mJ/m². Because carbon disulfide interactions are only dispersive ($\gamma_{CS_2} = \gamma_{CS_2}^{LW}$), Adamson *et al.*'s data [27, 47] can be used to calculate γ_{ice}^{LW} via the Young-Dupr'e Equation [48] and a geometric mean [49]

$$W_a^{LW} = \gamma_{CS_2} (1 + \cos \theta) = 2 \sqrt{\gamma_{ice}^{LW} \gamma_{CS_2}} \quad (5)$$

by taking temperature dependent values of γ_{CS_2} from the literature [50]. This shows that γ_{ice}^{LW} linearly decreases from 32.5 to 29.5 mJ/m² between 253 and 263 K, i.e. $\Delta \gamma_{ice}^{LW} = 3.0$ mJ/m². Thus, the majority of $\Delta \gamma_{ice}^{tot} \approx 16$ mJ/m² must be due to $\Delta \gamma_{ice}^{AB} \approx 13 \pm 2$ mJ/m², which is strikingly similar to $\Delta \gamma_{ice}^{AB} = 12.4$ mJ/m² measured by van Oss *et al.* [29], showing that there is a transition in γ_{ice}^{AB} at 257 K. Because the second molecular bilayer premelts at slightly different temperatures on different crystal faces [20], we expect γ_{ice}^{AB} of different faces to transition at slightly different temperatures. The difference in these temperatures is so close (1.7 K) that the methods used in this study are unlikely to be able to detect a difference in the γ_{ice}^{AB} transition temperature.

Until now, the premelting of ice has been linked to macroscopic phenomena only through the gradual increasing mobility of the top-most surface molecules. Our results show that there is also a change in the acid-base

component of the surface free energy of ice at the same temperature at which the second molecular bilayer premelts. This transition has ramifications in many areas. Roberts and Richardson saw a drastic decrease in both friction and pull-off adhesion force of polyisoprene on ice [35], both of which can be explained by the drop in surface energy of ice around 257 K. A similar transition seems plausible in the fracture toughness of ice [51]. The structure and surface energy of the premelt layer of ice is expected to have an influence on crystal growth from the vapor phase, which would influence the morphology of snowflakes [52]. Interestingly, the morphologies of snowflakes transition from long, slender columns to large, thin plates when the temperature reaches about 258 K [53], possibly due to γ_{ice}^{AB} transitioning at slightly different temperatures on different crystal faces.

In summary, we have shown that the thermodynamic work of adhesion between PDMS and ice drastically transitions at 257 K, the temperature at which the second molecular bilayer of the ice surface premelts. Unlike the ice-air interface, SFG spectra of both the PDMS surface and ice-PDMS interface show no sharp transition around 257 K, confirming that the transition in adhesion is due to a transition of the ice surface. Using contact angle data of carbon disulfide (capable of only dispersive interactions) on ice, we have shown that it is the acid-base component of the ice surface which show a transition of $\Delta\gamma_{ice}^{AB} \approx 13 \pm 2$ mJ/m². There is also pinning of the advancing contact line above 258 K, possibly due to energy dissipation in the mobility of the premelted bilayers. Understanding how the molecular structure of the premelt layer dictates the surface energetics of ice has direct implications for many scientific fields, from physicists aiming to understand adhesion and friction to biologists unraveling the mechanisms behind antifreeze proteins.

We thank Siddhesh Dalvi for the fabrication of the PDMS caps and Edward Laughlin for the design and construction of the SFG cooling stage. Insightful comments on the results were graciously provided by Manoj Chaudhury and Michael C. Wilson. We would also like to thank Amanda J. Stefin for reviewing the manuscript, and Mario Vargas and Andrew Work for discussions on the overall topic. Funding was provided by the National Science Foundation (NSF DMR-1610483) and the project was partially funded by a Goodyear Tire and Rubber Company fellowship.

* ali4@uakron.edu; blogs.uakron.edu/dhinojwala/

[1] I. K. Voets, *Soft Matter* **13**, 4808 (2017).

[2] B. N. Persson, *J. Chem. Phys.* **149**, 234701 (2018). [3] H. Trinks, W. Schröder, and C. K. Biebricher, *Orig. Life Evol. Biosph.* **35**, 429 (2005).

- [4] S. Li, P. G. Lucey, R. E. Milliken, P. O. Hayne, E. Fisher, J. P. Williams, D. M. Hurley, and R. C. Elphic, *Proc. Natl. Acad. Sci. U. S. A.* **115**, 8907 (2018).
- [5] C. M. Dundas, A. M. Bramson, L. Ojha, J. J. Wray, M. T. Mellon, S. Byrne, A. S. McEwen, N. E. Putzig, D. Viola, S. Sutton, E. Clark, and J. W. Holt, *Science*. **359**, 199 (2018).
- [6] Y. Cao, W. Tan, and Z. Wu, *Aerosp. Sci. Technol.* **75**, 353 (2018).
- [7] F. Afzal and M. S. Virk, *E3S Web Conf.* **72**, 01007 (2018).
- [8] E. Andenæs, B. P. Jelle, K. Ramlo, T. Kolås, J. Selj, and S. E. Foss, *Sol. Energy* **159**, 318 (2018).
- [9] M. Tomaszewski, B. Ruszczak, P. Michalski, and S. Zator, *Int. J. Crit. Infrastruct. Prot.* **25**, 139 (2019).
- [10] S. J. Lambert and B. K. Hansen, *Atmos. - Ocean* **49**, 289 (2011).
- [11] O. Lahayne, B. Pichler, R. Reihnsner, J. Eberhardsteiner, J. Suh, D. Kim, S. Nam, H. Paek, B. Lorenz, and B. N. Persson, *Tribol. Lett.* **62**, 1 (2016).
- [12] A. J. Tuononen, A. Kriston, and B. Persson, *J. Chem. Phys.* **145**, 114703 (2016).
- [13] M. Faraday, *J. Franklin Institute, State Pennsylvania, Promot. Mech. Arts; Devoted to Mech. Phys. Sci. Civ. Eng. Arts Manuf. Rec. Am. Other Pat. Invent.* **20**, 283 (1850).
- [14] B. Slater and A. Michaelides, *Nat. Rev. Chem.* **3**, 172 (2019).
- [15] X. D. Zhu, H. Suhr, and Y. R. Shen, *Phys. Rev. B* **35**, 3047 (1987).
- [16] A. G. Lambert, P. B. Davies, and D. J. Neivandt, *Appl. Spectrosc. Rev.* **40**, 103 (2005).
- [17] Y. R. Shen, *J. Phys. Chem. C* **116**, 15505 (2012).
- [18] X. Wei, P. B. Miranda, and Y. R. Shen, *Phys. Rev. Lett.* **86**, 1554 (2001).
- [19] X. Wei, P. B. Miranda, C. Zhang, and Y. R. Shen, *Phys. Rev. B* **66**, 085401 (2002).
- [20] M. Alejandra Sañchez, T. Kling, T. Ishiyama, M. J. Van Zadel, P. J. Bisson, M. Mezger, M. N. Jochum, J. D. Cyran, W. J. Smit, H. J. Bakker, M. J. Shultz, A. Morita, D. Donadio, Y. Nagata, M. Bonn, and E. H. Backus, *Proc. Natl. Acad. Sci. U. S. A.* **114**, 227 (2017).
- [21] S. Yamaguchi, Y. Suzuki, Y. Nojima, and T. Otsu, *Chem. Phys.* **522**, 199 (2019).
- [22] B. Weber, Y. Nagata, S. Ketzetzi, F. Tang, W. J. Smit, H. J. Bakker, E. H. Backus, M. Bonn, and D. Bonn, *J. Phys. Chem. Lett.* **9**, 2838 (2018).
- [23] J. F. D. Liljeblad, I. Furo, and E. C. Tyrode, *Phys. Chem. Chem. Phys.* **19**, 305 (2017).
- [24] A. Work and Y. Lian, *Prog. Aerosp. Sci.* **98**, 1 (2018).
- [25] Y. Nagata, T. Hama, E. H. Backus, M. Mezger, D. Bonn, M. Bonn, and G. Sazaki, *Acc. Chem. Res.* **52**, 1006 (2019).
- [26] F. M. Fowkes, *J. Phys. Chem.* **66**, 382 (1962).
- [27] A. W. Adamson, F. P. Shirley, and K. T. Kunichika, *J. Colloid Interface Sci.* **34**, 461 (1970).
- [28] J. Kloubek, *J. Colloid Interface Sci.* **46**, 185 (1974).
- [29] C. J. van Oss, R. F. Giese, R. Wentzek, J. Norris, and E. M. Chuvilin, *J. Adhes. Sci. Technol.* **6**, 503 (1992).

- [30] W. M. Ketcham and P. V. Hobbs, *Philos. Mag.* **19**, 1161 (1969).
- [31] L. B. Boinovich and A. M. Emelyanenko, *Dokl. Phys. Chem.* **459**, 198 (2014).
- [32] Y. Qiu and V. Molinero, *J. Phys. Chem. Lett.* **9**, 5179 (2018).
- [33] K. L. Johnson, K. Kendall, and A. D. Roberts, *Proc. R. Soc. A Math. Phys. Eng. Sci.* **324**, 301 (1971).
- [34] A. Dupr' e and P. Dupr' e, *Th' eorie m' ecanique de la chaleur* (1869).
- [35] A. D. Roberts and J. C. Richardson, *Wear* **67**, 55 (1981).
- [36] S. Dalvi, A. Gujrati, S. R. Khanal, L. Pastewka, A. Dhinojwala, and T. D. B. Jacobs, *Proc. Natl. Acad. Sci. U. S. A.* **116**, 25484 (2019).
- [37] K. Golovin, A. Dhyani, M. D. Thouless, and A. Tuteja, *Science* **364**, 371 (2019).
- [38] Y. Zhuo, F. Wang, S. Xiao, J. He, and Z. Zhang, *ACS Omega* **3**, 10139 (2018).
- [39] P. Irajizad, A. Al-Bayati, B. Eslami, T. Shafquat, M. Nazari, P. Jafari, V. Kashyap, A. Masoudi, D. Araya, and H. Ghasemi, *Mater. Horizons* **6**, 758 (2019).
- [40] M. Rubinstein and R. H. Colby, *Polymer Physics* (Oxford University Press, 2003).
- [41] B. Yurdumakan, G. P. Harp, M. Tsige, and A. Dhinojwala, *Langmuir* **21**, 10316 (2005).
- [42] C. Kim, M. C. Gurau, P. S. Cremer, and H. Yu, *Langmuir* **24**, 10155 (2008).
- [43] K. Nanjundiah, P. Y. Hsu, and A. Dhinojwala, *J. Chem. Phys.* **130**, 024702 (2009).
- [44] Q. Shi, S. Ye, S. A. Spanninga, Y. Su, Z. Jiang, and Z. Chen, *Soft Matter* **5**, 3487 (2009).
- [45] E. Anim-Danso, Y. Zhang, A. Alizadeh, and A. Dhinojwala, *J. Am. Chem. Soc.* **135**, 2734 (2013).
- [46] S. Wu, *J. Polym. Sci. Part C Polym. Symp.* **34**, 19 (1971).
- [47] A. Rohatgi, *WebPlotDigitizer* (2015).
- [48] N. K. Adam, *Nature* **180**, 809 (1957).
- [49] L. A. Girifalco and R. J. Good, *J. Phys. Chem.* **61**, 904 (1957).
- [50] N. A. Lange and J. A. J. A. Dean, *Lange's Handbook of chemistry*, rev. 10th ed. (McGraw-Hill, New York, 1979).
- [51] W. Nixon and E. Schulson, *J. Phys. Colloq.* **48**, 313 (1987).
- [52] K. G. Libbrecht, *A Quantitative Physical Model of the Snow Crystal Morphology Diagram*, Tech. Rep. (2019). [53] K. G. Libbrecht, *Reports Prog. Phys.* **68**, 855 (2005).